Saez-Ferre, S.; Boronat Zaragoza, M.; Cantin Sanz, A.; Rey Garcia, F.; Oña-Burgos, P. (26-0). Elucidation of the Interaction Mechanism between Organic Chiral Cages with Biomolecules through Nuclear Magnetic Resonance and Theoretical Studies. The Journal of Physical Chemistry C. 122(29):16821-16829. https://doi.org/10.1021/acs.jpcc.8b05069

THE JOURNAL OF PHYSICAL CHEMISTRY C

C: Surfaces, Interfaces, Porous Materials, and Catalysis

Elucidation of the Interaction Mechanism between Organic Chiral Cages with Biomolecules through Nuclear Magnetic Resonance and Theoretical Studies

Sara Sáez-Ferre, Mercedes Boronat, Angel Cantin, Fernando Rey, and Pascual Oña-Burgos

J. Phys. Chem. C, **Just Accepted Manuscript** • DOI: 10.1021/acs.jpcc.8b05069 • Publication Date (Web): 02 Jul 2018

Elucidation of the Interaction Mechanism between Organic Chiral Cages with Biomolecules through Nuclear Magnetic Resonance and Theoretical Studies

Sara Sáez-Ferre, Mercedes Boronat, Ángel Cantín, Fernando Rey* and Pascual Oña-Burgos*

Instituto de Tecnología Química, Universitat Politècnica de València-Consejo Superior de Investigaciones Científicas (UPV-CSIC), Avda. de los Naranjos s/n, 46022 Valencia, Spain.

Supporting Information Placeholder

ABSTRACT: A multinuclear NMR has been carried out to elucidate the mechanism of action of CC3-*R* box type chiral materials for the separation of enantiomers, supported by theoretical calculations. The potential of these materials to be used as chiral resolution agents through NMR is evidence in this study.

INTRODUCTION

Enantiomers have physical and chemical identical properties except for optical rotation, and they also have different biological and pharmacological properties. Therefore, chiral discrimination has become more important in several fields, as in the pharmaceutical industry, in stereospecific synthesis, in the food industry, environmental science and development of optical devices.[1-2] However, the separation of enantiomers is still a challenge due to their physical and chemical identical properties.

Microporous small pore size crystalline materials have been of great scientific and technological interest because of their potential applications in gas storage, heterogeneous catalysis and molecular separation. Most microporous solids are formed by extended three-directional networks such as, zeolites,[3-5] metal-organic frameworks (MOFs),[6-11] covalent-organic frameworks (COFs)[12-14] or organic polymer networks.[15-16]

Contrary to extended networks, porous organic molecular solids (POMs) can be soluble in organic solvents. The solubility of POMs offers some advantages in comparison to insoluble networks materials. Their monomers retain the same structural porosity as the original POMs after dissolution in common organic solvents, and are easily recrystallized. These POMs seem to open new avenues for promising further applications.

On this regards, the Cooper research's group synthesized a new class of porous organic cages (POCs) with permanent and available cavities formed via condensation reaction of 1,3,5-triformylbenzene or tris(4-formylphenyl)amine and various diamines and evidenced the cage-cage self-assemble into crystalline materials with permanent void space.[17-24] Cooper and co-workers first reported the synthesis of POC (CC3) and its use for chiral separation.[19,23]

CC3 is an imine-linked POC, which is synthesized by the one-step [4+6] condensation of 1,3,5-triformylbenzene with (*R*,*R*)-1,2-Diaminocyclohexane or (*S*,*S*)-1,2-Diaminocyclohexane. This cage has tetrahedral symmetry, and each cage has four windows, the cage molecules pack in a window-to-window arrangement that self-assemble into perfectly ordered materials. Porous organic molecular cages defined as shape-persistent three-dimensional organic molecules have been explored for gas adsorption, separation, molecular recognition and sensing. More recently, CC3-*R* has been used in gas-chromatographic (GC) separation. Particularly, CC3-*R* has been successfully used in the enantiomeric resolution of a wide variety of racemates belonging to different classes without derivatization.[25-26]

However, these relevant results are based on trial and error experiments and so far for being trivial, which racemates can be successfully resolved by a given chiral solid. Therefore, the development of physico-chemical techniques that can be used as screening for the mentioned separations could be of interest for many researchers working in pharmacy, separation, NMR, modelling, etc. For instance, there is little insight on the detailed interaction between the host CC3-*R* entity and the guest molecule. To best knowledge, there is just one report applying to a chiral molecule (1-phenyl-1-ethanol), where racemic mixture of 1-phenyl-1-ethanol is eluted through the chiral material and 30 % ee of the opposite configuration is obtained in the solution.

Within this study, we provide information related to the interaction of the material CC3-*R* with several small chiral organic molecules, many of them biomolecules. Furthermore, it is determined the preference of this material to some functional group, then we have found the application to separate racemic mixture of amino acids (*aa*) and alpha hydroxyl-acids (*ha*). In addition, we suggest that these materials are also likely to be used as resolution agents of enantiomers.

EXPERIMENTAL

General considerations: CC3-*R* and CC3-*S* were prepared according to literature procedures (or modified procedures) using solvothermal strategy.[21] The employed guests were purchased from Sigma–Aldrich and used without further purification. The samples for liquid NMR analysis were prepared as follows. CC3-*R* is dissolved in CD_2Cl_2 at 2.5 mM. Then the guest were added to this solution to achieve a final concentration of 1, 3, 10 mM for each sample.

Solution NMR spectroscopy: Solution NMR spectra were recorded with Bruker Avance instruments operating at ^{1}H Larmor frequency of 300 MHz. Chemical shifts are given in ppm and relative to TMS for ^{1}H and ^{13}C and relative to NH_3 (liquid) for ^{15}N nuclei. Coupling constants (J) are given in Hertz as positive values regardless of their real individual signs. PGSE NMR diffusion measurements were carried out by using the stimulated echo pulse

sequence.[27] A rectangular shape was used for the gradient pulses and their strengths changed automatically during the course of the experiments. The D values were determined from the slope of the regression line ln (I/I_0) versus G^2, according to Equation 1. I/I_0=observed spin echo intensity/intensity without gradients, G=gradient strength, Δ=delay between the midpoints of the gradients, D=diffusion coefficient, δ=gradient length. The measurements were performed without spinning. The calibration of the gradients was carried out by means of a diffusion measurement of HDO in D_2O (D_{HDO}=1.902 10^9 m^2 s^{-1}).[28] The experimental error in D values was estimated to be smaller than ±2% (three standard deviations). All of the data that led to the reported D values afforded lines with correlation coefficients above 0.999. The gradient strength was incremented in 8% steps from 10% to 98%, so that, depending on the signal/noise ratio, 10–12 points could be used for regression analysis. Afterwards, the Einstein-Stokes formula (equation 2) correlates D with hydrodynamic radius r_H.

Equation 1:

$$\ln(I/I_o) = -(\gamma\delta)^2 G^2 D(\Delta - \delta/3)$$

Equation 2: Einstein-Stokes formula

$$r_H = \frac{k\,T}{6\,\pi\,\eta\,D}$$

X-ray diffraction: The crystallinity of the materials was investigated by Powder X-ray diffraction (PXRD). The measurements were performed using a Panalytical X´Pert PRO diffractometer in a Bragg-Brentano geometry and Cu Kα1 radiation (λ = 1.5406 Å).

Other techniques: The morphology of the cages was analyzed by scanning electron microscopy (SEM). SEM micrographs were recorded on a SU8230 FE-SEM instrument working at 5–10 kV, using beam deceleration mode. The samples were prepared by placing a small amount of powder on a carbon tape on SEM stubs.C, N and H contents of isolated catalysts were determined with a Carlo Erba 1106 elemental analyzer. TGA analysis was carried out using a Mettler Toledo TGA/SDTA851e with an automated vertical overhead thermobalance.

DFT studies: All calculations in this work are based on density functional theory (DFT) and were carried out using the M062X functional[29] and the 6-311g(d,p) basis set,[30] as implemented in the Gaussian09 software.[31] The geometry of all structures was fully optimized without restrictions. Host-guest interaction energies were calculated as:

$$E_{int} = E(\text{host-guest}) - E(\text{host}) - E(\text{guest})$$

where E(host-guest) is the total energy of the complexes shown in Figures 5 and S83, and E(host) and E(guest) are the total energies of the isolated host model and guest molecules, respectively.

RESULTS

The CC3-*R* material was synthesized using solvothermal conditions. First of all, it was fully characterized by NMR. In fact, diffusion NMR spectroscopy was employed with the aim of measuring diffusion coefficients and estimating hydrodynamic radii of molecules in isotropic media.[32-33] This technique is mostly used to study organometallic complexes, as well as supramolecular systems such as host–guest systems, helicates, grids, supramolecular polymers and more. Diffusion NMR has also found applications in studies of biosystems, pharmaceutical ones and those of the structure of nanoparticles.[34-40] It is accepted that the diffusion decrease and the hydrodynamic radius of any species increases as the interaction with the host molecule increase. Therefore, this technique is especially well suited for studying host-guest interactions such as those occurring during adsorption and separation processes.

Pulsed Gradient Spin-Echo (PGSE) NMR diffusion measurements were used to determine the diffusion coefficients (D) of the material CC3-*R* studied here in solution (more details of these experiments are provided in the Supporting Information). The experiments were performed in CD_2Cl_2 from 0.25 to 2.5 mM concentrations of material in order to determine if agglomeration takes place. In table 1 the diffusion data and hydrodynamic radius for CC3-*R* are summarized and compared with the radius obtained from X-ray. The results shown in Table 1 indicate that diffusion (D) and hydrodynamic radius of CC3-*R* remain constant along the whole range of concentration, indicating that there is no agglomeration of the monomers for further experiments.

Table 1. Diffusion data for CC3-*R*.

Entry	[CC3-R] mM	D [10^{-10} m^2s^{-1}][a]	r_H [Å][b]	r_X [Å][c]
1	0.25 mM *R*	6.6	8.1	8.5
2	0.75 mM *R*	6.6	8.1	
3	2.5 mM *R*	6.6	8.1	

a) Experimental error in the D values was (± 2)%. b) The viscosity (η) used in the Stokes–Einstein equation was 0.410 10^{-3} $kgm^{-1}s^{-1}$. Values of η were taken from http://www.knovel.com. c) It is an estimation, deduced from the X-ray structure described in the reference 8.

NMR spectroscopy study of host–guest interactions. Intrigued by the way of action of materials in exerting the separation of organic molecules and racemates shown above, we propose a full study based on solution NMR that provide a direct and detailed view on the underlying interactions at the molecular level. Solution NMR spectroscopy could provide such a view since intermolecular interactions can be studied through their effect on the chemical shift, relaxation times and translational diffusion coefficients of the various species. In the case of protein receptors and ligand binding, specific NMR approaches are routinely applied to provide information about the binding process and conformations. Taking advantage of the presence of the permanent porosity of CC3-R material, its high organic content and its solubility in dichloromethane, we propose NMR-based approaches in host-guest heterogeneous related system for the *in situ* characterization of the molecular interactions.

First of all, we carried out ^{1}H NMR measurements of the POCs and the different guests at 298K with concentrations between 1 and 10mM in CD_2Cl_2. The solvent chosen is CD_2Cl_2 because the CC3 materials are fully soluble in this solvent. A number of guests have been employed in order to carry out this study including, 1-phenyl-ethylamine which Cooper used in his work, other biomolecules derived from protected amino acids in the amino group (Figure 1). For this study, free amino acids were not directly used because of their insolubility in CD_2Cl_2. Then, the corresponding commercially available BOC derivated chiral systems in their two enantiomeric forms have been selected, as shown in Figure 1. Then, it was carried out the measurement of the different samples constituted by the host, CC3-*R*, and each guest at different concentrations.

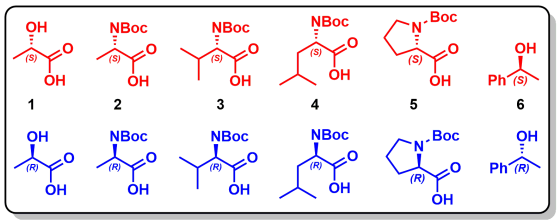

Figure 1. Illustration of the selected guests (L/S red and D/R blue).

First of all, both the host and the series of guests were studies at 298K as solution of pure compounds at 10 mM concentration in CD_2Cl_2. Then, the mixture of each guest (concentrations range from 1-10 mM) and the host (concentration of 2.5 mM) were also measured at 298K in CD_2Cl_2. In Table 2 the data of these measurements are collected through proton NMR, where the three signals of the COF H_1 (imine), H_2 (aromatic) and H_3 (α-*N*CH) are analyzed, with the purpose of studying the effect that the presence of different guests used at different concentrations has on the selected ^{1}H-NMR resonances of the host CC3-*R*, which is at a fixed concentration of 2.5 mM (Figure 2).

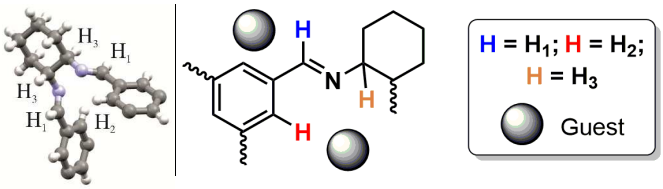

Figure 2. Illustration of the three selected signals of CC3-*R*.

The observed changes in chemical shifts for the three selected COF signals are shown in the right column (Guest@COF - COF). There, it is observed that the coupling of lactic acid (compound **1** in Figure 1 with CC3-*R* material (entries 2-7) produces a deshielding of the three characteristic resonances of the COF as evidence by the displacement towards higher δ of the ^{1}H NMR signal. The deshielding effect is more pronounced as the concentration of lactic acid increases. But more importantly, there is a stronger interaction between the CC3-*R* and *S* enantiomers that CC3-*R*. This phenomenon is clearly illustrated in the Figure 3.

Table 2. ^{1}H NMR data for the 3 selected signals of the host.

Entry	[guest] mM	δ ^{1}H NMR (ppm)			Δδ $H_1/H_2/H_3$
		H_1	H_2	H_3	
1	--	8.165	7.891	3.38	--/--/--
2	1mM *L*-**1**	8.165	7.891	3.381	0.000/0.000/0.001
3	3mM *L*-**1**	8.168	7.907	3.397	0.003/0.016/0.017
4	10mM *L*-**1**	8.176	7.935	3.428	0.011/0.044/0.048
5	1mM *D*-**1**	8.165	7.893	3.382	0.000/0.002/0.002
6	3mM *D*-**1**	8.166	7.900	3.390	0.001/0.011/0.010
7	10mM *D*-**1**	8.173	7.926	3.416	0.008/0.035/0.036
8	1mM *L*-**2**	8.167	7.894	3.385	0.002/0.003/0.005
9	3mM *L*-**2**	8.168	7.899	3.391	0.003/0.008/0.011
10	10mM *L*-**2**	8.167	7.904	3.400	0.002/0.013/0.020
11	1mM *D*-**2**	8.165	7.890	3.379	0.000/0.001/0.001
12	3mM *D*-**2**	8.165	7.895	3.385	0.000/0.004/0.005
13	10mM *D*-**2**	8.165	7.902	3.396	0.000/0.011/0.016
14	1mM *L*-**3**	8.165	7.890	3.379	0.000/-0.001/0.001
15	3mM *L*-**3**	8.165	7.896	3.386	0.000/0.005/0.006
16	10mM *L*-**3**	8.171	7.918	3.409	0.006/0.027/0.029
17	1mM *D*-**3**	8.165	7.891	3.381	0.000/0.000/0.001
18	3mM *D*-**3**	8.166	7.894	3.385	0.001/0.003/0.005
19	10mM *D*-**3**	8.168	7.910	3.400	0.003/0.019/0.020
20	1mM *L*-**4**	8.167	7.894	3.384	0.002/0.003/0.004
21	3mM *L*-**4**	8.167	7.897	3.389	0.002/0.006/0.009
22	10mM *L*-**4**	8.167	7.899	3.392	0.002/0.008/0.012
23	1mM *D*-**4**	8.166	7.891	3.380	0.001/0.000/0.000
24	3mM *D*-**4**	8.167	7.895	3.386	0.002/0.004/0.004
25	10mM *D*-**4**	8.165	7.897	3.388	0.000/0.006/0.008
26	1mM *L*-**5**	8.165	7.890	3.379	0.000/-0.001/0.001
27	3mM *L*-**5**	8.165	7.891	3.380	0.000/0.000/0.000
28	10mM *L*-**5**	8.166	7.894	3.386	0.001/0.003/0.006
29	1mM *D*-**5**	8.166	7.891	3.380	0.001/0.000/0.000
30	3mM *D*-**5**	8.166	7.892	3.382	0.001/0.001/0.002
31	10mM *D*-**5**	8.165	7.893	3.385	0.000/0.002/0.005
32	10mM *S*-**6**	8.162	7.889	3.378	0.003/0.003/0.002
33	10mM *R*-**6**	8.162	7.889	3.377	0.003/0.003/0.003

The guest **2** (*N*-Boc-alanine, inputs 8-13), **3** (*N*-Boc-valine, inputs 14-19 and **4** (*N*-Boc-leucine, inputs 20-25) have a similar behavior as described for ligand **1**. However, it is less import when the steric effect of the hydrophobic chain is enhanced. In this sense, this effect is slight for guest **5** (*N*-Boc-proline, inputs 26-31), where only few little changes in the signals of interest are detected for concentrations of 10mM, and the greatest effect is shown for the *L* series. Furthermore, as the size of the amino acid aliphatic chain increase, the effect on the host fades. Finally, guest **6** (1-phenylethanol, inputs 32-33) has no effect on guest signals in the range of 1- 10mM.

Moreover, if we analyze the data according to the absolute configuration of the host CC3-*R* used we can observe how the *L* series (*S* absolute configuration) produces a greater effect than the *D* series (R absolute configuration. However, the shift of ^{1}H NMR signal for experiments of guests 5@CC3-R (entries 26-31) is only observed for the highest guest concentration (10mM, entries 28 and 31), whilst no significant changes in the NMR signals are observed at lower concentration. Therefore, we can conclude that CC3-*R* material has a stronger affinity for carboxylic acid group than the *S* enantiomer. In addition, this affinity can be nicely modulated by controlling the steric volume of the aliphatic substituent.

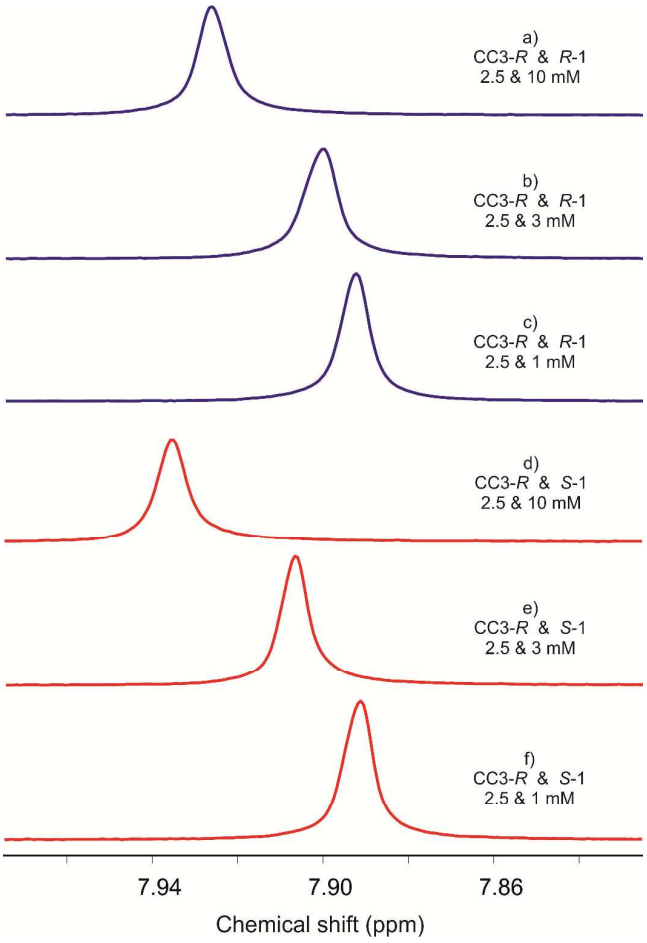

Figure 3. ^{1}H NMR data for H_2 signal of the host with both enantiomers of ligand 1 at several concentrations.

A deep study for assessing the binding of guest molecules and the host CC3-*R* was performed by applying ^{1}H,^{15}N gHMQC and ^{1}H,^{13}C gHSQC NMR experiments. These spectroscopic techniques have been used for understanding the structure–activity relationships (SAR) in biomolecules and proteins. In this sense,

NMR spectroscopy is employed to detect binding of drugs to receptor proteins and more important to identify the unit of the protein involved in the process. For instance, $^{1}H,^{15}N$ gHSQC or HMQC experiments were known to provide an effective method to investigate interactions of the guanidinium groups of arginine units with charged groups on the ligand.[41-47] Another experimental setup to detect binding of ligands to receptor proteins involves the acquisition of $^{1}H,^{13}C$ gHMQC spectra of probes with and without ligands present. Generally, labeling of proteins with ^{13}C is more expensive than with ^{15}N. Furthermore, $^{1}H,^{13}C$ gHSQC spectra are more complex than $^{1}H,^{15}N$ gHSQC spectra. Hence, $^{1}H,^{13}C$ gHSQC experiments have not been widely employed to test for binding. Nevertheless, in our case it is not a problem since our host-guest spectra have less signals. Therefore, both experiments were used to demonstrate the interaction between the CC3-*R* host and the selected molecules. One $^{1}H,^{15}N$ gHMQC experiment and other of $^{1}H,^{13}C$ gHSQC of the organic cage CC3-*R* are acquired as the reference spectra. Then, samples that contain one of the selected molecules (**1-6**) are prepared. If the resonance position of a cross-peak is significantly shifted compared to the reference spectra this is an indication of binding (SAR by NMR).

Table 3 shows the carbon-13 NMR data of two signals of the CC3-*R* C_1 (imine), C_2 (aromatic) and the nitrogen-15 data for the N_1 signal (imine) with the presence of the different guests used at different concentrations, keeping the concentration of the host at 2.5 mM. In addition, in the column on the right, the observed changes in the chemical shifts are shown for the three signals, two of carbon and one of nitrogen, of the host-isolated relative to the corresponding guest-host mix. The close analysis of the data collected in table 3 indicates that the change in C_1 and C_2 are very small, suggesting that the interaction between CC3-*R* and selected guests does not take place through the carbon atoms of the host, and therefore nitrogen atoms must be involved.

Table 3. ^{13}C and ^{15}N NMR data for the selected nuclei of the host.

Entry	[guest] mM	δ ^{13}C NMR (ppm)		δ ^{15}N NMR (ppm)	Δδ $C_1/C_2/N_3$
		C_1	C_2	N_3	
1	--	158.65	129.03	341.3	--/--/--
2	3mM *L*-**1**	159.10	129.20	338.7	0.45/0.17/2.60
3	10mM *L*-**1**	159.10	129.40	337.3	0.45/0.37/4.00
4	3mM *D*-**1**	159.00	129.13	339.4	0.35/0.10/1.90
5	10mM *D*-**1**	159.18	129.48	337.6	0.53/0.45/3.70
6	3mM *L*-**2**	158.8	129.20	339.5	0.15/0.17/1.80
7	10mM *L*-**2**	158.9	129.30	338.6	0.25/0.27/2.70
8	3mM *D*-**2**	158.65	129.09	340.0	0.00/0.06/1.30
9	10mM *D*-**2**	158.94	129.33	339.3	0.29/0.30/2.00
10	3mM *L*-**3**	158.80	129.15	339.8	0.15/0.12/1.50
11	10mM *L*-**3**	159.00	129.30	338.2	0.35/0.27/3.10
12	3mM *D*-**3**	158.78	129.11	340.4	0.13/0.08/0.90
13	10mM *D*-**3**	159.80	129.13	339.1	0.15/0.10/2.20
14	3mM *L*-**4**	158.94	129.13	340.9	0.29/0.10/0.40
25	10mM *L*-**4**	159.00	129.32	339.6	0.34/0.29/1.70
16	3mM *D*-**4**	158.86	129.06	341.2	0.21/0.03/0.10
17	10mM *D*-**4**	158.96	129.27	340.3	0.31/0.24/1.00
18	3mM *L*-**5**	158.65	129.09	341.0	0.00/0.06/0.30
19	10mM *L*-**5**	158.80	129.20	340.4	0.15/0.17/0.90
20	3mM *D*-**5**	158.74	129.03	341.6	0.09/0.00/0.30
21	10mM *D*-**5**	158.80	129.11	340.6	0.15/0.08/0.70
22	10mM *S*-**6**	158.69	129.06	341.0	0.04/0.03/0.30
23	10mM *R*-**6**	158.67	129.04	341.1	0.02/0.01/0.20

Indeed, the changes in the chemical shift of nitrogen are quite significant with the presence of the guests **1-5** indicating that a strong interaction host-guest occurs in good agreement with the observed shifts in ^{1}H NMR signals. Meanwhile, there is practically no effect in the NMR signals when molecule **6** is adsorbed. In addition, the observed changes for **1-4** are in line with what is observed for the proton, where at 3 and 10 mM guest concentrations changes are detected in host signals. Moreover, the effect is higher for *L* series. However, at guest **5** this is only observed at concentrations of 10 mM, and in all cases slightly higher for the *L*. This behaviour evidences the interactions between both systems through the carboxylic group and the steric effect of the hydrophobic chain decrease this interaction.

After that, it was decided to study the effect that the presence of the host has on guest signals. Table 4 summarizes the proton data between the guest-free and the guest-CC3-*R*, maintaining the concentration of CC3-*R* at 2.5 mM and that of the guest at 3 and 10 mM. The associated changes are in line with those observed in the CC3-*R*. The major changes are those associated with ligand **1** (entries 1-5), and especially the *L* series, in all cases the signals are shielded. Ligand **2** (entries 6-10) also presents more significant changes for the *L* than for the *D* series, this change being of shielding towards the methynic proton and deshielding towards the methyl group. However, for ligands **3-5** (entries 11-23) deshielding happens in all of them, and these deshieldings are greater for the *L* than for the *D* series. All these data can be summed up as: 1) large steric effect of the guest enhances the deshielding of its ^{1}H NMR signals; 2) large affinity of the guest to the host minimized the deshielding of guest ^{1}H NMR signals. Therefore, this supports why this effect is lower in the *D* series. On the other hand, the proton signals corresponding to ligand **6** (entries 24-26) do not show any significant changes, so neither the guest nor the host are affected. This reinforces the finding that the interaction takes place through the carboxylic acid.

Table 4. ^{1}H NMR data for the selected signals of the ligands 1-6 at several concentrations and the host at 2.5mM concentration.

Entry	[guest] mM	**CC3-R** mM	δ ^{1}H NMR (ppm)		Δδ H_1/H_2
			H_1	H_2	
1	*L*-**1**	--	4.388	1.488	
2	3mM *L*-**1**	2.5	4.3512	1.4863	0.0365/0.0017
3	10mM *L*-**1**	2.5	4.311	1.4428	0.077/0.0452
4	3mM *D*-**1**	2.5	4.3622	1.4865	0.0258/0.0015
5	10mM *D*-**1**	2.5	4.351	1.4718	0.037/0.0165
6	*L*-**2**	--	4.2914	1.44	
7	3mM *L*-**2**	2.5	4.2861	1.4413	0.0053/-0.0013
8	10mM *L*-**2**	2.5	4.2808	1.4474	0.0106/-0.074
9	3mM *D*-**2**	2.5	4.2905	1.4420	0.0009/-0.0020
10	10mM *D*-**2**	2.5	4.2866	1.4415	0.0048//-0.0015
11	*L*-**3**	--	4.2086	1.0246/ 0.96	
12	3mM *L*-**3**	2.5	4.208	1.0375/ 0.9709	0.0006/-0.0129/ -0.0109
13	10mM *L*-**3**	2.5	4.1815	1.0235/ 0.9604	0.0271/0.0011/ -0.0004
14	3mM *D*-**3**	2.5	4.2080	1.0369/ 0.9649	0.0006/-0.0123/ -0.0049
15	10mM *D*-**3**	2.5	4.1765	1.0148/ 0.9461	0.0321/0.0098/ 0.0139
16	*L*-**4**	--	4.264	0.9836/ 0.9757	
17	3mM *L*-**4**	2.5	4.278	1.004/ 0.9917	-0.014/-0.0204/ -0.016
18	10mM *L*-**4**	2.5	4.278	1.0098/ 0.9966	-0.014/-0.0262/ -0.0209
19	3mM *D*-**4**	2.5	4.278	0.9962	-0.014/-0.0126/ -0.0205
20	10mM *D*-**4**	2.5	4.278	1.0036	-0.014/-0.02/ -0.0279
21	*L*-**5**	--	4.352	--	
22	10mM *L*-**5**	2.5	4.344	--	0.008
23	10mM *D*-**5**	2.5	4.350	--	0.002
24	10mM *S*-**6**	--	4.902	1.490	

25	10mM *S*-**6**	2.5	4.911	1.491	-0.007/-0.001
26	10mM *R*-**6**	2.5	4.911	1.490	-0.007/0.000

Figure 4 shows the ^{1}H-NMR spectra of the CC3-*R* in presence of the guest 1 in its *L*, *R* and racemic forms. There, we can observe that the material CC3-*R* is not only a good support of chiral column for gas and liquid chromatography for the separation of enantiomeric mixtures as has been shown in previous studies, but it could also act as a chiral solvating agent (CSA) for poorly impeded *N*-BOC-aminoacids and α-hydroxy acids. Therefore, this material would have an even wider application than that reported so far.

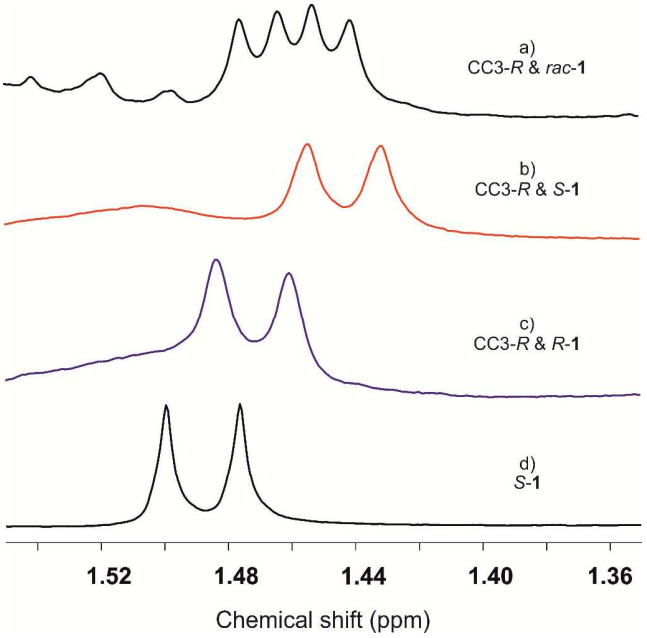

Figure 4. ^{1}H NMR region for the corresponding methyl group signal of ligand 1 at 3 mM and the host at 2.5mM; a) *rac*-1; b) *S*-1; c) *R*-1; d) isolated *S*-1.

A variety of NMR pulse sequences that allow the investigation of diffusion constants in solution has been applied to understand the host-guest interaction and diffusion in CC3-*R*. On the basis of such experiments it is possible to discriminate compounds in mixtures according to their diffusion properties. This diffusion experiment has been previously successfully applied to deconvolute compound mixtures, and to detect molecular association processes.[48-53] Although, the main difficulty is that for the detection of changes in the diffusion constant of a ligand that binds to a protein, it is necessary that a significant amount of the ligand is bound to the protein on the time average. Diffusion experiments have been proven to be a valuable tool for characterizing molecular interactions between small and intermediate size molecules. Therefore, PGSE diffusion NMR has been also applied to the several samples. Then, the preparation of different samples of the selected guests with and without CC3-*R* present was carried out and then the comparison of the corresponding diffusion constant should give information about the binding affinity.

Table 5 shows the data obtained from the diffusion measurements on all the guests in the samples at a concentration of 2.5 and 3 mM for the host and guest, respectively. As in previous studies, the case of lactic acid has been the most relevant, confirming that the enantiomer *L* has a slightly higher affinity than the *D* enantiomer towards the guest CC3-*R*. The changes in the diffusion coefficients and hydrodynamic radius are very clear between free host and host-guest. In fact, more than 50% of *L*-lactic acid is interacting with the host material. On the other hand, changes in the values of the diffusion coefficients and hydrodynamic radii for the other guests **2**-**6** are not very significant, being at best 21% host, *L*-**2**, which interacts with the guest very far from the values determined for *L*-**1**.

Table 5. Diffusion data for the selected guests 1-7 with and without the host.

Entry	[guest] 3mM	COF 2.5mM	D 10^{-10} m^2/s	r_H Å	guest free/guest inside
1	--	X	6.6	8.1	
2	*L*-**1**	--	22.3	2.4	
3	*L*-**1**	X	13.5	3.9	51.6/48.4
4	*D*-**1**	X	14.2	3.7	56.1/43.9
5	*L*-**2**	--	14	3.8	
6	*L*-**2**	X	12.4	4.3	78.2/21.8
7	*D*-**2**	X	12.8	4.2	83.8/16.2
8	*L*-**3**	--	13.1	4.1	
9	*L*-**3**	X	12.3	4.3	87.7/12.3
10	*D*-**3**	X	12.8	4.2	91.4/8.6
11	*L*-**4**	--	13.1	4.1	
12	*L*-**4**	X	12.2	4.4	86.2/13.8
13	*D*-**4**	X	12.4	4.3	89.2/10.8
14	*L*-**5**	--	15	3.5	
15	*L*-**5**	X	14.5	3.7	94/6
16	*D*-**5**	X	14.9	3.6	98.8/1.2
17	*S*-**6**	--	22.3	2.4	
18	*S*-**6**	X	21.1	2.5	95.5/4.5
19	*R*-**6**	X	21.6	2.5	94.9/5.1

Finally, Saturation-transfer NMR spectroscopy, STD, has been used for many years to characterize binding in tightly bound ligand-receptor complexes. At the same time it was also shown that STD NMR is an excellent technique for determining the binding epitope of the ligand, information that is of prime importance for the directed development of drugs.[54] Based on that, STD experiments were carried out over several samples, because it is a suitable experiment to probe SAR by NMR spectroscopy, and also to determine association/dissociation contacts. However, STD experiments were not successful since the size of the host is too small for applying these experiments being applicable for systems larger than 15000 KDa.

DFT study of host–guest interactions.

The interaction of guest molecules **1** and **2** and benzoic acid with a porous organic cage of composition $N_{12}C_{72}H_{84}$ as a model of the CC3-*R* material were theoretically investigated by means of DFT calculations. After full geometry optimization without any restriction, the organic cage maintains its tetrahedral symmetry as well as its window size and shape. The interaction of lactic acid **1** with the CC3-R model involves a strong hydrogen bond between the proton of the carboxylic group of the guest molecule and the imine N atom of the host POC and, in some cases, an additional weaker interaction between the C=O oxygen atom of lactic acid and a neighbouring imine H_1 atom (see Figure 5). And the same type of adsorption is found for the guest molecule alanine **2**. For both molecules, different adsorption complexes can be obtained depending on the relative orientation of the methyl group of the guest with respect to the organic skeleton of the host COF. All calculated interaction energies range from -60 to -80 kJ/mol, and the relative stability of the two most stable orientations for each enantiomer (labelled as **a** or **b** in Figure 5 and Table 6) differ by 15 kJ/mol at most. It is also important to remark that the interaction of the CC3-*R* model with the *L* enantiomer is in both systems slightly stronger than with the *D* enantiomer, in agreement with the results from the NMR study.

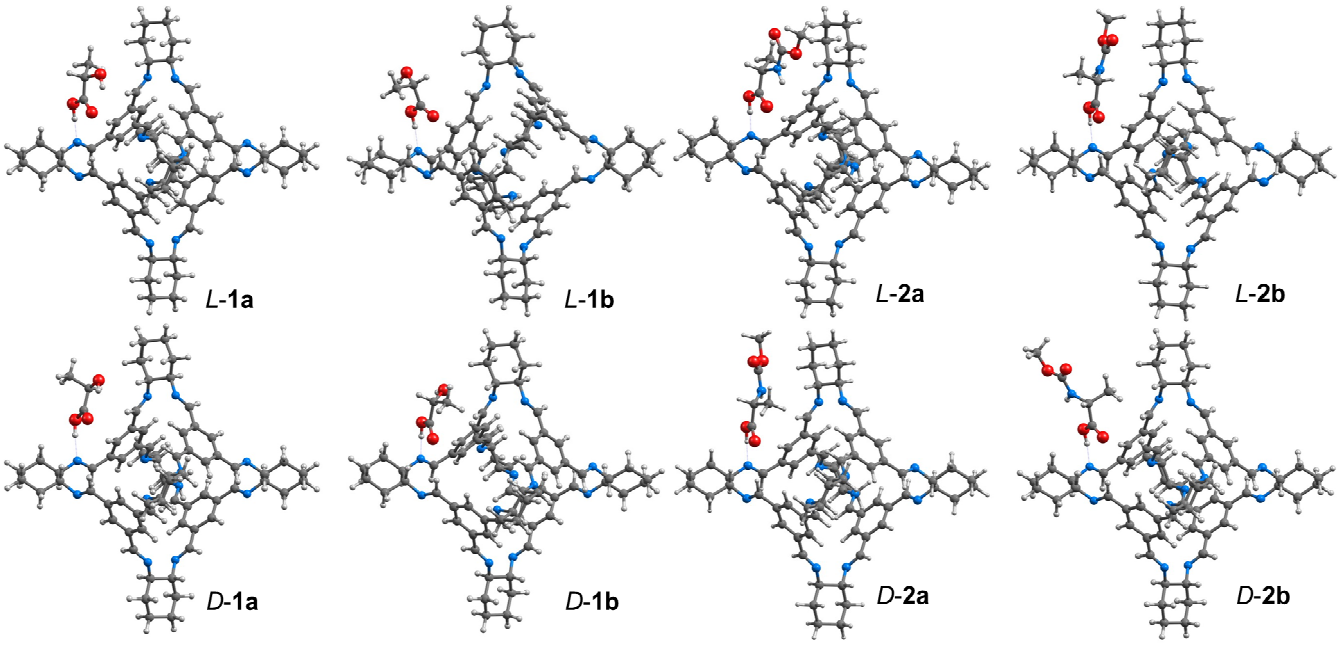

Figure 5. DFT structures for the interaction CC3-*R*-guest; a) *L*-1 and *D*-1; b) *L*-2 and *D*-2.

Finally, the interaction of benzoic acid with the CC3-*R* model by π interaction between aromatic rings was also considered, and compared with the previously described carboxylic group-imine bonding (see Figure S83 of the SI). The calculated interaction energies, -44.6 and -77.4 kJ/mol for the π and imine bonding, respectively, confirm the preferential interaction through the carboxylic group.

Changes in the chemical shifts and an increase in signal line widths are observed in the ^{1}H NMR spectrum of the host for *N*-BOC-aminoacids and especially with the α-hydroxy acid. This effect implies a greater deshielding of signals of CC3-*R* towards those hosts with more affinity. When the alcohol **6** was studied no change in the chemical shift of the signals with respect to the isolated species was observed. This behaviour evidences the interactions between both systems through the carboxylic group. Likewise, the ^{1}H NMR signals of the hosts in the presence of the guest also suffer displacements of the signals with respect to the free compound. Further shielding of such signals is related to a greater affinity towards the guest by the host. Other functional groups, such as free amino acids, were not able to be studied since CC3-*R* is only slightly soluble in CD_2Cl_2 while free amino acids are only soluble in D_2O or polar organic solvent. In the study carried out by means of carbon NMR on the signals of the CC3-*R* imine and aromatic it has been shown that this nucleus undergoes very small changes of magnitude and therefore does not provide great information as sensor of the interaction process. However, the nitrogen NMR provides a great deal of information and could be considered an indicator of the degree of host-guest interaction.

Table 6. DFT data for the host-guest systems depicted in the Figure 5.

Entry	Guest	E_{int} kJ/mol	$r_{H\text{-}H1}$ Å	$r_{H\text{-}H2}$ Å	$r_{H\text{-}H3}$ Å
1	*L*-**1a**	-76.9	2.519	3.540	2.838
2	*L*-**1b**	-61.6	3.933	4.191	4.669
3	*D*-**1a**	-74.8	2.923	3.633	3.414
4	*D*-**1b**	-69.3	2.464	3.764	2.671
5	*L*-**2a**	-78.9	2.548	3.451	2.837
6	*L*-**2b**	-73.0	2.450	3.549	2.836
7	*D*-**2a**	-72.7	2.265	3.631	2.512
8	*D*-**2b**	-63.7	2.552	3.788	2.654

In addition, NMR diffusion can also be established as a very useful tool to identify that molecules interact more strongly with these chiral boxes. All these results were supported with theoretical calculations. Finally, the possibility of using these materials as chiral resolution agents by NMR has been opened.

CONCLUSION

In summary, the study carried out on the CC3-*R* systems, through NMR and supported by theoretical calculations, has allowed to elucidate and to understand the interactions of these systems with different hosts. In addition, it becomes clear that NMR is a very useful technique to identify such mechanism of action, guest-host interaction, in enantiomeric separation processes, just as it has been in biology. Finally, it has been determined that such materials can be used as enantiomeric resolution agents by NMR. Currently, we are working to develop chiral materials that act on CSA but with a greater capacity for the determination of enantiomeric excesses.

ASSOCIATED CONTENT

Supporting Information

The Supporting Information is available free of charge on the ACS Publications website. Experimental procedures, spectral and computational details (PDF). Cartesian coordinates for all optimized structures (XYZ).

AUTHOR INFORMATION

Corresponding Author

* F.R. Email: frey@itq.upv.es
* P. O-B. Email: pasoabur@itq.upv.es

Notes

The authors declare no competing financial interest.

ACKNOWLEDGMENT

Program Severo Ochoa SEV-2016-0683 is gratefully acknowledged. S.S-F. thanks MEC for his Severo Ochoa Grant SPV-2013-067884, P. O-B. thanks MEC for his Ramón y Cajal contract RYC-2014-16620. M. B and F.R thank the financial support by the Spanish Government (MAT2017-82288-C2-1-P and MAT2015-71842-P). The Electron Microscopy Service of the UPV is acknowledged for their help in sample characterization.

REFERENCES

(1) Pu, L. Enantioselective fluorescent sensors: a tale of BINOL. *Acc. Chem. Res.* **2012**, *45*, 150-163.
(2) Zhang, X.; Yin, J.; Yoon, J. Recent advances in development of chiral fluorescent and colorimetric sensors. *Chem. Rev.* **2014**, *114*, 4918-4959.
(3) Simancas, R.; Dari, D.; Velamazán, N.; Navarro, M. T.; Cantín, A.; Jordá, J. L.; Sastre, G.; Corma, A.; Rey, F. Modular organic structure-directing agents for the synthesis of zeolites. *Science* **2010**, *330*, 1219.
(4) Moliner, M.; Martínez, C.; Corma, A. Synthesis strategies for preparing useful small pore zeolites and zeotypes for gas separations and catalysis. *Chem. Mater.* **2014**, *26*, 246-258.
(5) Moliner, M.; Martínez, C.; Corma , A. Multipore zeolites: synthesis and catalytic applications. *Angew. Chem. Int. Ed.* **2015**, *54*, 3560-3579.
(6) Corma, A.; García, H.; Llabrés i Xamena, F. X. Engineering metal organic frameworks for heterogeneous catalysis. *Chem. Rev.* **2010**, *110*, 4606-4655.
(7) Dhakshinamoorthy, A.; Opanasenko, M.; Cejka, J.; Garcia, H. Metal organic frameworks as heterogeneous catalysts for the production of fine chemicals. *Catal. Sci. Technol.* **2013**, *3*, 2509-2540.
(8) Valvekens, P.; Vermoortele, F.; De Vos, D. Metal–organic frameworks as catalysts: the role of metal active sites. *Catal. Sci. Technol.* **2013**, *3*, 1435-1445.
(9) Jiang, J.; Yaghi, O. M. Brønsted acidity in metal–organic frameworks. *Chem. Rev.* **2015**, *115*, 6966-6997.
(10) Seoane, B.; Castellanos, S.; Dikhtiarenko, A.; Kapteijn, F.; Gascon, J. Multi-scale crystal engineering of metal organic frameworks. *Coord. Chem. Rev.* **2016**, *307*, 147-187.
(11) Chen, L.; Luque, R.; Li, Y. Controllable design of tunable nanostructures inside metal-organic frameworks. *Chem. Soc. Rev.* **2017**, *46*, 4614-4630.
(12) Zhang, Y.-B.; Su, J.; Furukawa, H.; Yun, Y.; Gándara, F.; Duong, A.; Zou, X.; Yaghi, O. M. Single-crystal structure of a covalent organic framework. *J. Am. Chem. Soc.* **2013**, *135*, 16336-16339.
(13) Díaz, U.; Corma, A. Ordered covalent organic frameworks, COFs and PAFs. From preparation to application. *Coord. Chem. Rev.* **2016**, *311*, 85-124.
(14) Das, S.; Heasman, P.; Ben, T.; Qiu, S. Porous organic materials: strategic design and structure–function correlation. *Chem. Rev.* **2017**, *117*, 1515-1563.
(15) Dawson, R.; Cooper, A. I.; Adams, D. J. Nanoporous organic polymer networks. *Prog. Polym. Sci.* **2012**, *37*, 530-563.
(16) Tan, L.; Tan, B. Hypercrosslinked porous polymer materials: design, synthesis, and applications. *Chem. Soc. Rev.* **2017**, *46*, 3322-3356.
(17) Bojdys, M. J.; Hasell, T.; Severin, N.; Jelfs, K. E.; Rabe, J. P.; Cooper, A. I. Porous organic cage crystals: characterising the porous crystal surface. *Chem. Commun.* **2012**, *48*, 11948-11950.
(18) Tozawa, T.; Jones, J. T. A.; Swamy, S. I.; Jiang, S.; Adams, D. J.; Shakespeare, S.; Clowes, R.; Bradshaw, D.; Hasell, T.; Chong, S. Y.; Tang, C.; Thompson, S.; Parker, J.; Trewin, A.; Bacsa, J.; Slawin, A. M. Z.; Steiner, A.; Cooper, A. I. Porous organic cages. *Nat. Mater.* **2009**, *8*, 973-978.
(19) Chen, L.; Reiss, P. S.; Chong, S. Y.; Holden, D.; Jelfs, K. E.; Hasell, T.; Little, M. A.; Kewley, A.; Briggs, M. E.; Stephenson, A.; Thomas, K. M.; Armstrong, J. A.; Bell, J.; Busto, J.; Noel, R.; Liu, J.; Strachan, D. M.; Thallapally, P. K.; Cooper, A. I. Separation of rare gases and chiral molecules by selective binding in porous organic cages. *Nat. Mater.* **2014**, *13*, 954-960.
(20) Briggs, M. E.; Slater, A. G.; Lunt, N.; Jiang, S.; Little, M. A.; Greenaway, R. L.; Hasell, T.; Battilocchio, C.; Ley, S. V.; Cooper, A. I. Dynamic flow synthesis of porous organic cages. *Chem. Commun.* **2015**, *51*, 17390-17393.
(21) Jiang, S.; Jones, J. T. A.; Hasell, T.; Blythe, C. E.; Adams, D. J.; Trewin, A.; Cooper, A. I. Porous organic molecular solids by dynamic covalent scrambling. *Nat. Commun.* **2011**, *2*, 207.
(22) Little, M. A.; Chong, S. Y.; Schmidtmann, M.; Hasell, T.; Cooper, A. I. Guest control of structure in porous organic cages. *Chem. Commun.* **2014**, *50*, 9465-9468.
(23) Kewley, A.; Stephenson, A.; Chen, L.; Briggs, M. E.; Hasell, T.; Cooper, A. I. Porous organic cages for gas chromatography separations. *Chem. Mater.* **2015**, *27*, 3207-3210.
(24) Briggs, M. E.; Cooper, A. I. A perspective on the synthesis, purification, and characterization of porous organic cages. *Chem. Mater.* **2017**, *29*, 149-157.
(25) Xie, S.-M.; Zhang, J.-H.; Fu, N.; Wang, B.-J.; Chen, L.; Yuan, L.-M. A chiral porous organic cage for molecular recognition using gas chromatography. *Anal. Chim. Acta* **2016**, *903*, 156-163.
(26) Zhang, J.-H.; Xie, S.-M.; Chen, L.; Wang, B.-J.; He, P.-G.; Yuan, L.-M. Homochiral porous organic cage with high selectivity for the separation of racemates in gas chromatography. *Anal. Chem.* **2015**, *87*, 7817-7824.
(27) Stilbs, P. *Prog. Nucl. Magn. Reson. Spectrosc.* **1987**, 19, 1-45.
(28) Tyrrell, H. J. V.; Harris, R. K. *Diffusion in Liquids, Butterworths*; London, 1984.
(29) Zhao, Y.; Truhlar, D. G. The M06 suite of density functionals for main group thermochemistry, thermochemical kinetics, noncovalent interactions, excited states, and transition elements: two new functionals and systematic testing of four M06-class functionals and 12 other functionals. *Theor. Chem. Acc.*, **2008**, *120*, 215–241.
(30) Raghavachari, K.; Binkley, J. S.; Seeger, R.; Pople, J. A. Self□consistent molecular orbital methods. XX. A basis set for correlated wave functions. *J. Chem. Phys.* **1980**, *72*, 650–654.
(31) Frisch, M. J.; Trucks, G. W.; Schlegel, H. B.; Scuseria, G. E.; Robb, M. A.; Cheeseman, J. R.; Scalmani, G.; Barone, V.; Petersson, G. A.; Nakatsuji, H.; et al. Gaussian 09, Revision C.01. Gaussian, Inc., Wallingford CT, 2009.
(32) Stejskal, E. O.; Tanner, J. E. Spin diffusion measurements: spin echoes in the presence of a time□dependent field gradient. *J. Chem. Phys.* **1965**, *42*, 288-292.
(33) Tanner, J. E. Use of the stimulated echo in NMR diffusion studies. *J. Chem. Phys.* **1970**, *52*, 2523-2526.
(34) Johnson, C. S. *Progress Nuc. Magn. Reson. Spect.* **1999**, *34*, 203-256.
(35) Chen, A.; Wu, D.; Johnson, C. S. Determination of molecular weight distributions for polymers by diffusion-ordered NMR. *J. Am. Chem. Soc.* **1995**, *117*, 7965-7970.
(36) Avram, L.; Cohen, Y. Diffusion NMR of molecular cages and capsules. *Chem. Soc. Rev.* **2015**, *44*, 586-602.
(37) Åslund, I.; Nowacka, A.; Nilsson, M.; Topgaard, D. Filter-exchange PGSE NMR determination of cell membrane permeability. *J. Magn. Reson.* **2009**, *200*, 291-295.
(38) Occhipinti, P.; Griffiths, P. C. Active targeting schemes for nanoparticle systems in cancer therapeutics. *Adv. Drug Deliv. Rev.* **2008**, *60*, 1570-1582.
(39) Marega, R.; Aroulmoji, V.; Dinon, F.; Vaccari, L.; Giordani, S.; Bianco, A.; Murano, E.; Prato, M. Diffusion-ordered NMR spectroscopy in the structural characterization of functionalized carbon nanotubes. *J. Am. Chem. Soc.* **2009**, *131*, 9086-9093.
(40) Canzi, G.; Mrse, A. A.; Kubiak, C. P. Diffusion-ordered NMR spectroscopy as a reliable alternative to TEM for determining the size of gold nanoparticles in organic solutions. *J. Phys. Chem. C* **2011**, *115*, 7972-7978.
(41) Pascal, S. M.; Yamazaki, T.; Singer, A. U.; Kay, L. E.; Forman-Kay, J. D. Structural and dynamic characterization of the phosphotyrosine binding region of an Src homology 2 domain-phosphopeptide complex by NMR relaxation, proton exchange, and chemical shift approaches. *Biochemistry* **1995**, *34*, 11353-11362.
(42) Yamazaki, T.; Pascal, S. M.; Singer, A. U.; Forman-Kay, J. D.; Kay, L. E. NMR pulse schemes for the sequence-specific assignment of arginine guanidino 15N and 1H chemical shifts in proteins. *J. Am. Chem. Soc.* **1995**, *117*, 3556-3564.

(43) Feng, M.-H.; Philippopoulos, M.; MacKerell, A. D.; Lim, C. Structural characterization of the phosphotyrosine binding region of a high-affinity SH2 domain−phosphopeptide complex by molecular dynamics simulation and chemical shift calculations. *J. Am. Chem. Soc.* **1996**, *118*, 11265-11277.
(44) Gargaro Angelo, R.; Frenkiel Thomas, A.; Nieto Pedro, M.; Birdsall, B.; Polshakov Vladimir, I.; Morgan William, D.; Feeney, J. NMR Detection of arginine□ligand interactions in complexes of lactobacillus casei dihydrofolate reductase. *Eur. J. Biochem.* **1996**, *238*, 435-439.
(45) Nieto, P. M.; Birdsall, B.; Morgan, W. D.; Frenkiel, T. A.; Gargaro, A. R.; Feeney, J. Correlated bond rotations in interactions of arginine residues with ligand carboxylate groups in protein ligand complexes. *FEBS Lett.* **1997**, *405*, 16-20.
(46) Morgan, W. D.; Birdsall, B.; Nieto, P. M.; Gargaro, A. R.; Feeney, J. H/15N HSQC NMR studies of ligand carboxylate group interactions with arginine residues in complexes of brodimoprim analogues and lactobacillus casei dihydrofolate reductase. *Biochemistry* **1999**, *38*, 2127-2134.
(47) Polshakov, V. I.; Morgan, W. D.; Birdsall, B.; Feeney, J. Validation of a new restraint docking method for solution structure determinations of protein–ligand complexes. *J. Biomol. NMR* **1999**, *14*, 115-122.
(48) Hajduk, P. J.; Olejniczak, E. T.; Fesik, S. W. One-dimensional relaxation- and diffusion-edited NMR methods for screening compounds that bind to macromolecules. *J. Am. Chem. Soc.* **1997**, *119*, 12257-12261.
(49) Lin, M.; Shapiro, M. J. mixture analysis in combinatorial chemistry. Application of diffusion-resolved NMR spectroscopy. *J. Org. Chem.* **1996**, *61*, 7617-7619.
(50) Lin, M.; Shapiro, M. J.; Wareing, J. R. Screening mixtures by affinity NMR. *J. Org. Chem.* **1997**, *62*, 8930-8931.
(51) Lin, M.; Shapiro, M. J.; Wareing, J. R. Diffusion-edited NMR−affinity NMR for direct observation of molecular interactions. *J. Am. Chem. Soc.* **1997**, *119*, 5249-5250.
(52) Bleicher, K.; Lin, M.; Shapiro, M. J.; Wareing, J. R. Diffusion edited NMR: Screening compound mixtures by affinity NMR to detect binding ligands to vancomycin. *J. Org. Chem.* **1998**, *63*, 8486-8490.
(53) Anderson, R. C.; Lin, M.; Shapiro, M. J. Affinity NMR: Decoding DNA binding. *J. Comb. Chem.* **1999**, *1*, 69-72.
(54) Mayer, M.; Meyer, B. Characterization of ligand binding by saturation transfer difference NMR spectroscopy. *Angew. Chem. Int. Ed.* **1999**, *38*, 1784-1788.

Insert Table of Contents artwork here

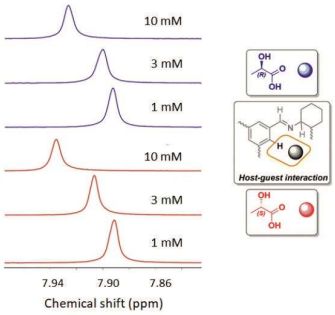

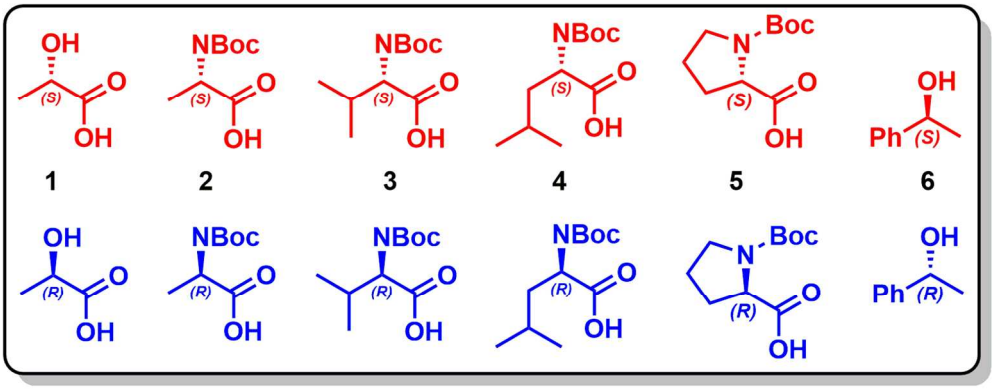

Figure 1. Illustration of the selected guests (L/S red and D/R blue).

134x52mm (300 x 300 DPI)

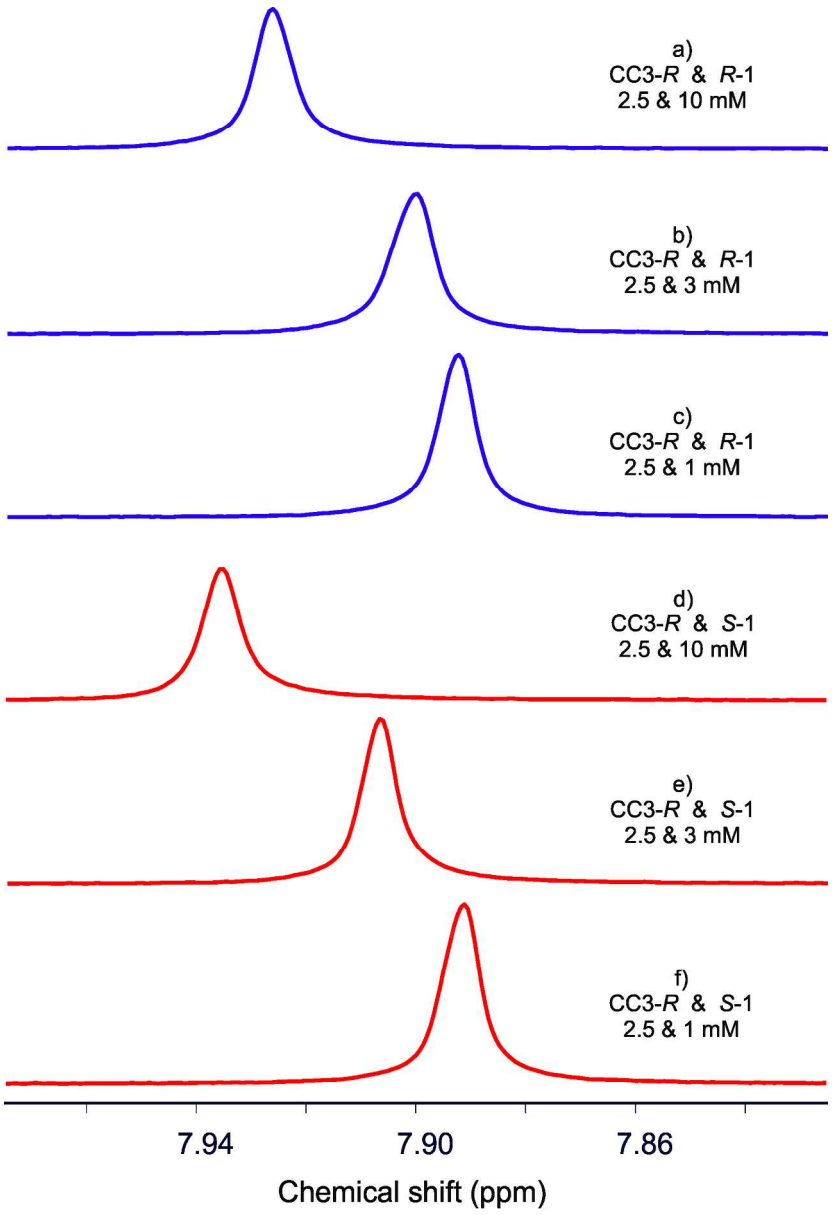

Figure 3. ^{1}H NMR data for H_2 signal of the host with both enantio-mers of ligand 1 at several concentrations.

179x261mm (300 x 300 DPI)

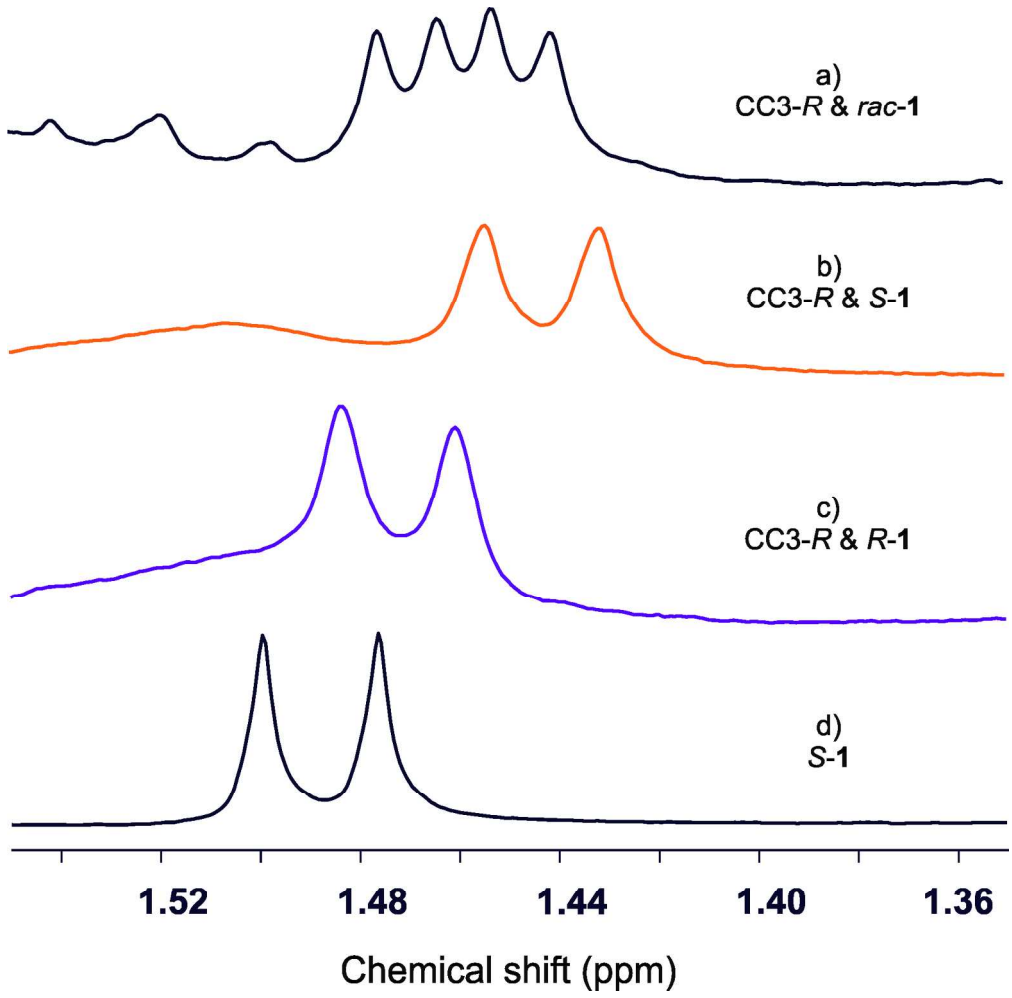

Figure 4. ^{1}H NMR region for the corresponding methyl group signal of ligand 1 at 3 mM and the host at 2.5mM; a) *rac*-1; b) *S*-1; c) *R*-1; d) isolated *S*-1.

173x170mm (300 x 300 DPI)

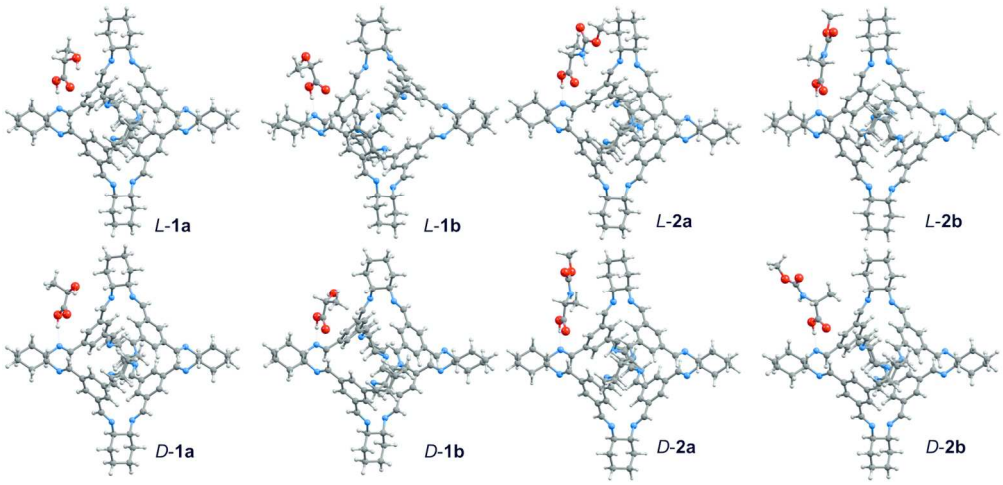

Figure 5. DFT structures for the interaction CC3-*R*-guest; a) *L*-1 and *D*-1; b) *L*-2 and *D*-2.

207x99mm (300 x 300 DPI)

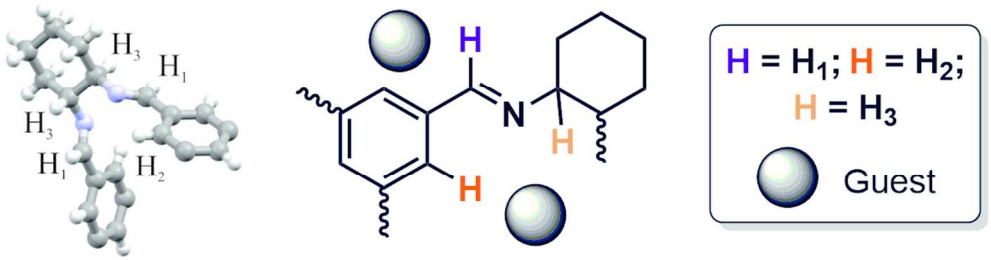

Figure 2. Illustration of the three selected signals of CC3-*R*.

101x26mm (300 x 300 DPI)

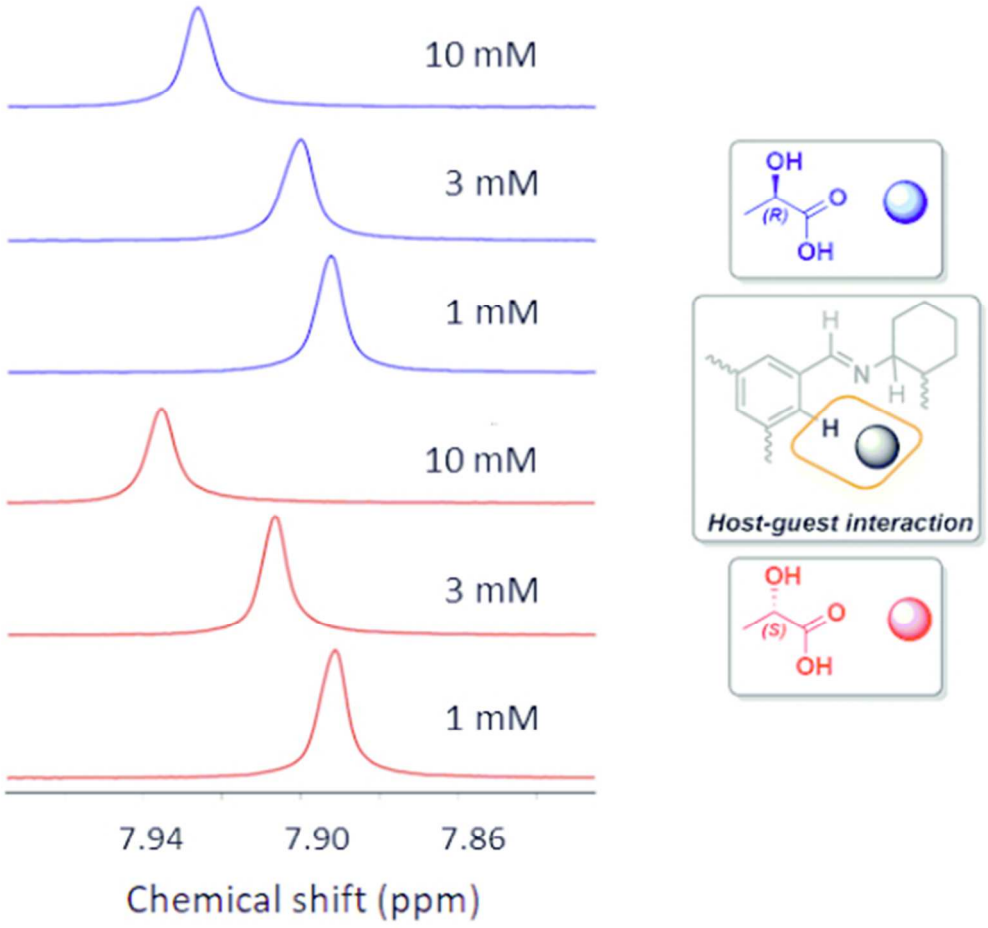

TOC graphic

46x44mm (300 x 300 DPI)